THE JOURNAL OF BIOLOGICAL CHEMISTRY VOL. 285, NO. 9, pp. 6848–6856, February 26, 2010

Filling the Gap, Evolutionarily Conserved Omp85 in Plastids of Chromalveolates*[S]

Received for publication, October 10, 2009, and in revised form, December 21, 2009 Published, JBC Papers in Press, December 30, 2009, DOI 10.1074/jbc.M109.074807

Lars Bullmann[‡], Raimund Haarmann[§], Oliver Mirus[§], Rolf Bredemeier[§], Franziska Hempel[‡], Uwe G. Maier[‡1], and Enrico Schleiff[§2]

From [‡]Cell Biology, Philipps-University Marburg, D-35032 Marburg, Germany and the [§]Cluster of Excellence Frankfurt and Center for Membrane Proteomics, Department of Biosciences, Molecular Cell Biology, Goethe University, D-60438 Frankfurt, Germany

Chromalveolates are a diverse group of protists that include many ecologically and medically relevant organisms such as diatoms and apicomplexan parasites. They possess plastids generally surrounded by four membranes, which evolved by engulfment of a red alga. Today, most plastid proteins must be imported, but many aspects of protein import into complex plastids are still cryptic. In particular, how proteins cross the third outermost membrane has remained unexplained. We identified a protein in the third outermost membrane of the diatom *Phaeodactylum tricornutum* with properties comparable to those of the Omp85 family. We demonstrate that the targeting route of *P. tricornutum* Omp85 parallels that of the translocation channel of the outer envelope membrane of chloroplasts, Toc75. In addition, the electrophysiological properties are similar to those of the Omp85 proteins involved in protein translocation. This supports the hypothesis that *P. tricornutum* Omp85 is involved in precursor protein translocation, which would close a gap in the fundamental understanding of the evolutionary origin and function of protein import in secondary plastids.

Many ecologically and medically relevant organisms such as diatoms, accounting for ~20% of worldwide primary production and CO_2 fixation (1), and the apicomplexan parasite *Plasmodium falciparum* (2) harbor multimembraned secondary plastids, which evolved by the engulfment and intracellular reduction of a red alga harboring a primary plastid by another eukaryotic cell. In diatoms, the secondary plastid is surrounded by four membranes. Here, the outermost membrane is in continuum with the host's endoplasmic reticulum (ER)[3] and therefore studded with 80 S ribosomes. The second membrane most likely represents the plasma membrane of the red algal endosymbiont, whereas the third and fourth membranes are homologous to the plastid envelope of the red alga's primary plastid (see Fig. 1*A*) (3, 4).

As in other phototrophic eukaryotes, the coding capacity of the genome of secondary plastids is reduced to a very limited number of genes. Therefore, most of the protein content is nucleus-encoded and has to be imported from the cytosolic compartment of the cell. In all secondarily evolved organisms investigated to date, nucleus-encoded plastid proteins are encoded as preproteins, in which a so-called bipartite targeting sequence (BTS) is found N-terminally (see Fig. 1*A*). This targeting sequence comprises a signal peptide and a further stretch of amino acids, called the transit peptide (see Fig. 1*A*) (3, 4). The N-terminal signal peptide portion of the BTS facilitates translocation into the ER lumen via the Sec61 translocon (see Fig. 1*A*) and is cleaved off afterward. This results in N-terminal exposure of the transit peptide, which mediates translocation across the remaining membranes. From the ER lumen, proteins are most likely translocated across the second membrane by a machinery that evolved from the endosymbiont's ER-associated protein degradation machinery, now referred to as SELMA (see Fig. 1*A*) (5), and are released into the periplastidal compartment (PPC), which is the remnant cytoplasm of the secondary endosymbiont. Further subplastidal targeting depends on the first amino acid of the transit peptide. An aromatic amino acid at the first position targets the protein into the stroma; otherwise, the proteins are retained in the PPC (6, 7). In the innermost membrane, components of a Tic complex (see Fig. 1*A*) were identified and shown to be involved in protein translocation (3, 4, 8). The translocon in the third outermost membrane remains to be identified, however.

According to morphology and evolution, the third outermost membrane might at least in part be functionally homologous to the outer membrane of plastids that originated by primary endosymbiosis. In the latter, cyanobacterial Omp85 is thought to have evolved into the general import pore of the outer membrane (9, 10), namely Toc75 (11, 12), as seen in all primary plastids investigated so far. Proteins of the Omp85 family are essential constituents of both bacteria and organelles, which originated from primary endosymbiosis (9, 10, 13, 14). Omp85-related proteins were initially discovered as surface-exposed antigen D15 and Oma87 from *Haemophilus influenza* (15) and *Pasteurella multocida* (16), respectively, and were shown to be excellent drug targets, correlating with their importance for the insertion of outer membrane proteins (17–24). Omp85 proteins are generally composed of an N-terminal POTRA domain and a C-terminal 16-stranded β-barrel (25, 26), but functional

* This work was supported by the Deutsche Forschungsgemeinschaft (SFB TR1/A10 (to O. M. and E. S.) and SFB807/P17 (to R. H. and E. S.)), the Volkswagenstiftung (to R. B. and E. S.), Graduate School 1216 (to L. B. and U. G. M.), and SFB 593 (to F. H. and U. G. M.).

[S] The on-line version of this article (available at http://www.jbc.org) contains supplemental Figs. 1–3.

[1] To whom correspondence may be addressed. E-mail: maier@staff.uni-marburg.de.

[2] To whom correspondence may be addressed. E-mail: schleiff@bio.uni-frankfurt.de.

[3] The abbreviations used are: ER, endoplasmic reticulum; BTS, bipartite targeting sequence; PPC, periplastidal compartment; *pt*Omp85, *P. tricornutum* Omp85; GFP, green fluorescent protein; MCS, multiple cloning site; MOPS, 4-morpholinepropanesulfonic acid.

distinctions exist among Omp85 proteins with respect to, for example, the pore-gating behavior or the pore size. For example, the proteobacterial/mitochondrial Omp85 proteins (referred to as the Sam50 type) have a considerably smaller pore diameter than the cyanobacterial/plastidal Omp85 proteins (referred to as the Toc75 type) (27). It is suggested that these differences might reflect distinct functional properties, as Sam50 is involved in mitochondrial outer membrane protein integration and Toc75 in the translocation of precursor proteins across membranes (*e.g.* Ref. 11). Hence, determination of electrophysiological properties serves as a tool to distinguish different Omp85 proteins.

Here, we report the discovery of an Omp85 homolog that is localized in the third outermost plastid membrane of the diatom *Phaeodactylum tricornutum*. Homologs of this Omp85 protein can be found in other secondarily evolved organisms of red algal ancestry. The *P. tricornutum* homolog has electrophysiochemical characteristics comparable with those of cyanobacterial Omp85 proteins and Toc75 from land plants. Therefore, we hypothesize that the Omp85 protein described here contributes to protein transport in complex plastids, thereby filling a gap in our understanding of protein import into and evolution of secondarily evolved organisms.

EXPERIMENTAL PROCEDURES

Structural Analysis—As templates for structural modeling of *P. tricornutum* Omp85 (*pt*Omp85), we used the crystal structures[4] of the POTRA domains of the Omp85 homolog Alr2269 from *Anabaena* sp. PCC 7120 (19) and of the β-barrel domain of the Omp85 homolog FhaC from *Bordetella pertussis* (26). (The final sequence alignment is shown in supplemental Fig. 1.) The templates were superimposed with the YASARA MUSTANG plug-in (28). By secondary structure prediction and a multiple alignment with several members of the Omp85 family from various species, including sequences from the marine metagenome project (29), we identified the POTRA domains in *pt*Omp85. In contrast, the β-barrel was hard to assign based on secondary structure prediction alone, which predicts many helical regions (*e.g.* PSIPRED) (30). Nevertheless, the multiple alignment described above enabled a clear identification of the β-barrel start, and the alignment was adjusted by including a careful manual analysis of a prediction of transmembrane β-strands (31). With Modeler Version 8.2 (32), we constructed an initial model of *pt*Omp85, which was refined with YASARA and its NOVA and YAMBER3 force fields (33). Side chains were optimized with SCWRL (34) as implemented in YASARA (SCWALL). The electrostatic potential of the pore was calculated with the Poisson-Boltzmann solvation model (35) with the AMBER99 force field (36). The negative (red) and positive (blue) electrostatic potential are mapped onto the surface of the pore with the exception of the conserved loop (residues 559–589) to illustrate the location of patches of positive/negative electrostatic potential. The maximum absolute electrostatic potential used for the color range of the protein surface is 100 kJ/mol.

[4] R. Haarmann, O. Mirus, and E. Schleiff, unpublished data.

Phylogenetic Analysis—Amino acid sequences of Omp85 from bacterial and eukaryotic species were obtained from GenBank™ (37). Sequences were aligned with the program MAFFT (version 6.708) (38). A maximum likelihood phylogeny was reconstructed with IQPNNI Version 3.3.1 (39). The accession numbers of the sequences used are given in Table 1, and the alignment is shown in supplemental Fig. 2. We constructed 1000 non-parametric bootstrap trees with IQPNNI and calculated the support values for the branches with TREE-PUZZLE (40).

Generation of Enhanced Green Fluorescent Protein Constructs—The full-length open reading frames of *pt*Omp85 and MGD1 (>estExt_gwp_gw1.C_chr_130058, Department of Energy Joint Genomic Institute) and the truncated *pt*Omp85 targeting sequences were amplified from cDNA and cloned into the pPha-T1 vector (41, 42) via a BamHI restriction site, upstream of the enhanced GFP coding sequence.

Generation of Self-assembling Split Green Fluorescent Protein (GFP) Constructs—Self-assembling split GFP fragments representing β-strands 1–10 and β-strand 11 of GFP (S1–10 and S11, respectively) are able to self-assemble and recover fluorescence only if present in the same cellular compartment (43). *pt*Omp85 was fused to S11, and the reporter was fused to S1–10 as detailed in Table 2. The respective fragments were engineered with convenient restriction sites for subsequent cloning into pPha-Dual (S1–10, 5′-NdeI + 3′-SacII; and S11, 5′-BamHI + 3′-SacII and 5′-NdeI + 3′-SacII). Open reading frames to be tested were amplified from cDNA using primers bearing appropriate 5′- and 3′-restriction sites. pPha-Dual carries two distinct multiple cloning sites (MCSs). MCS1 comprises restriction sites EcoRI and HindIII, and MCS2 comprises SpeI and SacII. Expression of cloned constructs is regulated via the light-inducible *fcpD* promotor (MCS1) and the NO_3-inducible nitrate reductase promotor (MCS2). The constructs used are listed in Table 2. *P. tricornutum* transformations were performed as described (41) with pPha-T1 and pPha-Dual plasmids containing the enhanced GFP and self-assembling split GFP constructs, respectively.

Fluorescence Microscopic Analysis—After transformation of *P. tricornutum*, fluorescence was monitored by confocal laser scanning microscopy on a Leica TCS SP2 microscope using HCX PL APO 40×/1.25-0.75 oil CS or PL APO 63×/1.32-0.60 oil Ph3 CS objectives. Fluorescence was excited at 488 nm, filtered with a beam splitter (TD 488/543/633), and detected by two different photomultiplier tubes with bandwidths of 500–520 and 625–720 nm for GFP and chlorophyll fluorescence, respectively.

ptOmp85 Targeting and Localization—*P. tricornutum* cells were harvested at 2500 × *g* for 10 min and resuspended in solubilizing buffer A (50 mM imidazole HCl (pH 7.5), 50 mM NaCl, 2 mM 6-aminocaproic acid, 1 mM EDTA, 8.5% sucrose, and protease inhibitor mixture). Cells were lysed by passing five times through a French press (Aminco) at 1000 p.s.i. Lysates were centrifuged again (4 °C, 8000 × *g*, 10 min) to remove intact cells and insoluble material. Membrane fractions were pelleted at 100,000 × *g* for 1 h. Membrane pellets were washed with carbonate buffer (100 mM $NaHCO_3$ (pH 11.5), 1 mM EDTA, and protease inhibitor mixture) to extract peripheral membrane

proteins and centrifuged again as described above. Carbonate-extracted membrane fractions were finally resuspended in solubilizing buffer A. Equal volumes of the soluble protein fraction, the carbonate-extracted peripheral membrane protein fraction, and the integral membrane protein fraction were treated with 15% trichloroacetic acid to precipitate proteins. Precipitated proteins were solubilized in equal volumes of urea buffer (8 mM urea, 200 mM Tris-HCl, 0.1 mM EDTA, 5% (w/v) SDS, 0.03% (w/v) bromphenol blue, and 1% (v/v) β-mercaptoethanol). Protein volumes equivalent to 15 μg of the membrane protein fraction were run on a 12.5% polyacrylamide gel, and proteins were transferred to nitrocellulose membrane, blocked with 5% skimmed milk powder in Tris-buffered saline/Tween, and probed with primary antibody (goat anti-GFP antibody (Roche Applied Science), 1:3000, in Tris-buffered saline/Tween and 5% skimmed milk powder). Membranes were washed in Tris-buffered saline/Tween and probed with horseradish peroxidase-conjugated rabbit anti-goat secondary antibodies (Clontech; 1:10,000, in Tris-buffered saline/Tween and 5% skimmed milk powder).

Electrophysiology—The coding sequence of mature *pt*Omp85 was amplified from *P. tricornutum* RNA with the OneStep RT-PCR kit (Qiagen, Hilden, Germany) and cloned into the pQE30 vector (Qiagen) encoding an N-terminal 6-His tag. Vectors were transformed into *Escherichia coli* BL21 cells, and expression was induced with 1 mM isopropyl β-D-thiogalactopyranoside at A_{600} = 1. Cells were lysed by sonification in 50 mM Tris (pH 8), 100 mM NaCl, 5 mM EDTA, 1 mM dithiothreitol, 0.5% (w/v) Triton X-100, 5 mM β-mercaptoethanol, and 2 mg/ml lysozyme. Inclusion bodies were pelleted by centrifugation at 15,000 rpm for 30 min at 4 °C and washed once with 20 mM Tris (pH 7.5), 200 mM NaCl, 10 mg/ml deoxycholic acid, 10 mg/ml Nonidet P-40, and 10 mM β-mercaptoethanol; twice with 20 mM Tris (pH 7.5), 1 mM EDTA, 0.5% (w/v) Triton X-100, and 5 mM β-mercaptoethanol; and finally with 20 mM Tris (pH 8), 1 mM EDTA, and 10 mM dithiothreitol. Subsequently, inclusion bodies were resolved in 8 M urea, 150 mM NaCl, and 50 mM sodium P_i, and protein was purified using nickel-nitrilotriacetic acid Superflow (Qiagen) and Mono S (GE Healthcare) with a gradient from 50 mM to 1 M NaCl in 20 mM Tris (pH 7) and 6 M urea. Reconstitution of the purified protein into liposomes and electrophysiological measurements were performed as described (27, 44).

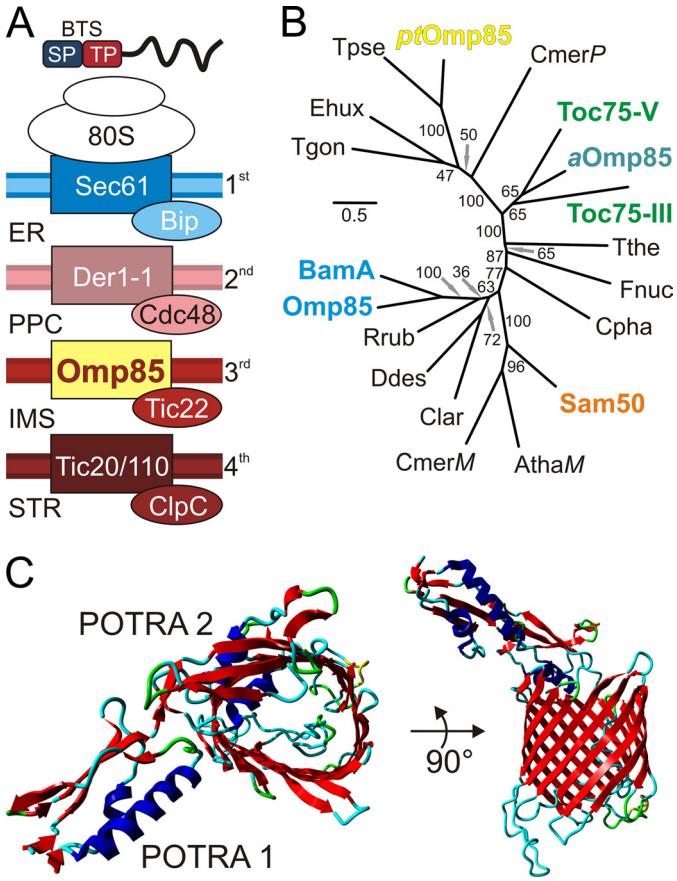

FIGURE 1. **An Omp85 homolog exists in complex plastids.** *A*, model of previously identified/suggested translocation components of each of the four membranes of complex plastids, including the Omp85 protein identified here. Secondary plastids of heterokontophytes are surrounded by four membranes. The first is in continuum with the ER (*blue*). The second membrane (*pink*) separates the PPC from the ER lumen. The intermembrane space (*IMS*) and the stroma (*STR*) are surrounded by the third (*red*) and fourth (*brown*) membranes, respectively. Nucleus-encoded plastid proteins (on *top*) possess a BTS at their N termini, which comprises a signal peptide (*SP*; *dark blue*) mediating cotranslational import via the Sec61 translocon. The transit peptide (*TP*; *red*) mediates translocation across the second membrane, most likely via the ER-associated protein degradation-derived SELMA complex. Stromal proteins bearing an aromatic amino acid at position +1 of the transit peptide are further translocated across the plastid envelope membranes by Omp85 (identified here) and by Tic20. *B*, calculation of phylogenetic relation of Omp85 proteins. Experimentally studied proteins from proteobacteria (*blue*), cyanobacteria (cyan), mitochondria (*orange*), and chloroplasts (*green*) and the *pt*Omp85 protein studied herein (*yellow*) are highlighted. The bootstrap values were calculated as described and are given in percent of support. *C*, top and side views of the homology model of *pt*Omp85.

RESULTS

Identification of ptOmp85—In the case of secondary plastids surrounded by four membranes, previous analyses have revealed putative protein translocons located in three of the four membranes (Fig. 1*A*) (3, 4, 8). We have identified a sequence in the genome of the diatom *P. tricornutum* with similarity to Omp85 (*pt*Omp85) (Fig. 1*B* and Table 1) (45). The N terminus of this protein is predicted to be a BTS for plastid import (3, 4). Structural modeling of *pt*Omp85 based on existing crystal structures (26) revealed a 16-stranded β-barrel and two POTRA domains (Fig. 1*C* and supplemental Fig. 1). The *pt*Omp85 sequence further enabled us to identify homologous protein sequences in the diatom *Thalassiosira pseudonana*, the haptophyte *Emiliania huxleyi*, and the apicomplexan parasites *Toxoplasma gondii* and *P. falciparum*. All of these homologs possess at least a predicted signal sequence (except *E. huxley*, in which the actual start codon is still unclear), the typical N-terminal POTRA signature, and a C terminus with probability to form a β-barrel.

We phylogenetically analyzed these sequences, together with proteo- and cyanobacterial Omp85, chloroplast Toc75, and mitochondrial Sam50/Tob55 proteins (Fig. 1*B*). (*P. falciparum* was excluded due to a biased amino acid composition resulting from the unusual high genomic AT content of *P. falciparum* (46).) In general, we observed the established branching of the Omp85 sequences (27). In particular, the chromalveolate Omp85 proteins branch together with cyanobacterial and chloroplast Omp85-like proteins rather than with mitochondrial/

TABLE 1

Sequences of the phylogenetic tree

Shown are names, species of origin, and accession number of sequences used for phylogenetic analysis. Accession numbers refer to the NCBI Database; numbers marked with single or double asterisks are from the *Emiliania huxleyi* Genome Database or the *Cyanidioschyzon merolae* Genome Project Database, respectively. aOmp85, *Anabaena* Omp85.

Name	Species	Accession no.
Tgon	*T. gondii*	gi 237833148
Ehux	*E. huxleyi*	fgeneshEH_pg.8_212/ fgeneshEH_pg.16_130*
Tpse	*T. pseudonana*	GU203520
*pt*Omp85	*P. tricornutum*	GU203519
CmerP	*C. merolae*	CMJ202C**
Toc75-V	*A. thaliana*	gi 18419973
aOmp85	*Anabaena* sp. PCC 7120	gi 17229761
Toc75-III	*A. thaliana*	gi 15232625
Tthe	*Thermus thermophilus*	gi 55980530
Fnuc	*Fusobacterium nucleatum*	gi 19705216
Cpha	*Chlorobium phaeobacteroides*	gi 67938686
Sam50	*Xenopus laevis*	gi 38014784
AthaM	*A. thaliana*	gi 18414910
CmerM	*C. merolae*	CMO061C**
Clar	*Campylobacter lari*	gi 57240748
Ddes	*Desulfovibrio desulfuricans*	gi 23475818
Rrub	*Rhodospirillum rubrum*	gi 48764608
Omp85	*Neisseria meningitidis*	gi 2460281
BamA	*E. coli*	gi 1786374
Pfal	*P. falciparum*	gi 124806499[a]

[a] Please note that the *P. falciparum* Omp85 homolog was excluded from the phylogenetic analyses due to an exceptional amino acid composition that results from the unusually high genomic AT content of *P. falciparum*.

proteobacterial ones. The closest affiliation was seen for the Toc75 protein from the free-living red alga *Cyanidioschyzon merolae*, indicating that chromalveolate Omp85 proteins are of the Toc75 type rather than the Sam50 type. The observed phylogenetic relation is very well supported with the exception of one split in the clade of proteobacteria and two splits between red algae and chromalveolates (Fig. 1*B*). This further strengthens the hypothesis that plastids of chromalveolates share an evolutionarily common origin (47).

Localization of ptOmp85—To further characterize the functionality of the predicted *pt*Omp85 BTS, we constructed a fusion of the full-length open reading frame to GFP. Such fusion constructs can be used to define the localization of proteins in *P. tricornutum* (Fig. 2*A*) (48). After transfecting the construct into *P. tricornutum*, a GFP signal was detected in the complex plastid (Fig. 2*B*, *first panel*), which accumulated in a region surrounding the plastid stroma. This localization is similar to that known from proteins targeted into the space between the second and third outermost membranes, the PPC (Fig. 2*A*) (48). By Western blot analyses of protein fractions from transfected *P. tricornutum* cells with anti-GFP antibodies, we confirmed that the fusion protein composed of the entire Omp85 protein was indeed integrated into a membrane (Fig. 2*C*). In contrast, a fusion protein of GFP and the BTS remained soluble, as did the control protein PsbO (Fig. 2*C*) (49).

Targeting of ptOmp85 Is Dependent on an Additional Signal—To further explore the targeting of the protein, we analyzed the BTS in detail. *pt*Omp85 possesses a phenylalanine at position +1 of the transit peptide, which is a signal for stromal import (6). However, the observed localization of the full-length protein was not stromal. Therefore, we hypothesized that *pt*Omp85 might be imported by a two-step mechanism as observed for the plant protein Toc75 (50). Toc75 possesses an N-terminal BTS composed of a "classical" transit peptide

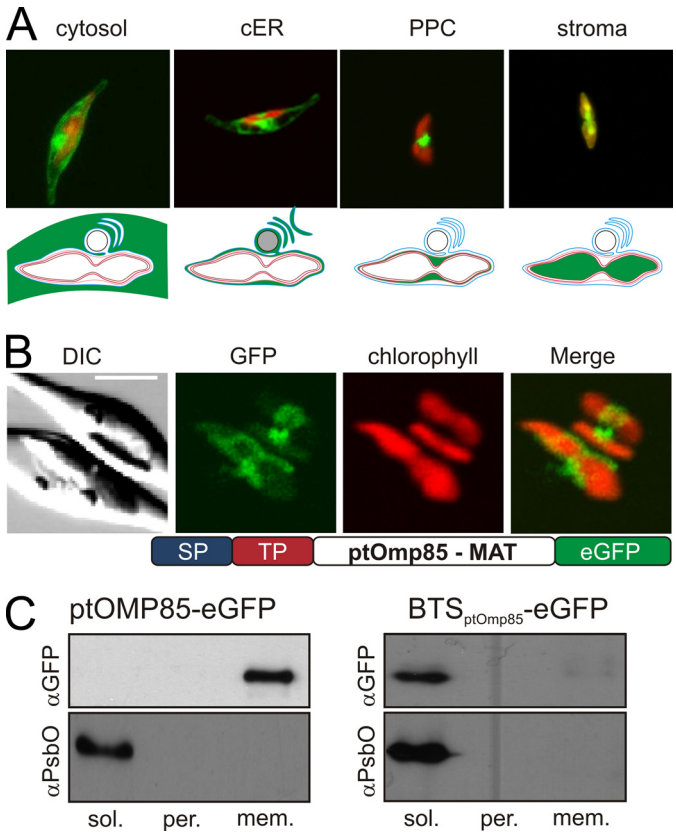

FIGURE 2. **Membrane localization of the Omp85-like protein in *P. tricornutum*.** *A*, distribution of GFP targeted to the cytoplasm, the ER lumen by fusion to the signal peptide of the ER luminal chaperone Bip (Bip-SP), PPC by fusion to the symbiontic Hsp70 BTS, and stroma by fusion to the AtpC BTS is shown for comparison. The *model* at the *bottom* shows the localization of GFP in the respective compartments of *P. tricornutum* to explain the GFP fluorescence. *B*, the full-length open reading frame of *pt*Omp85 fused to GFP was transfected into *P. tricornutum*. Cells expressing the construct show a green fluorescence inside the complex plastid surrounding the stroma. Shown are the differential interference contrast (*DIC*) image, GFP fluorescence, and chlorophyll fluorescence. *Merge* shows the overlay of chlorophyll and GFP fluorescence. *Scale bar* = 5 μm. *SP*, signal peptide; *TP*, transit peptide; *MAT*, mature protein; *eGFP*, enhanced GFP. *C*, *P. tricornutum* transfected with *pt*Omp85-GFP (*left*) or *pt*Omp85 BTS-GFP ($BTS_{ptOmp85}$-*GFP*; the 75 N-terminal amino acids fused to GFP) was separated into fractions representing soluble proteins (*sol.*), peripheral membrane proteins (*per.*), and integral membrane proteins (*mem.*). Fractions were analyzed by Western blotting with anti-GFP (*top*) or anti-PsbO (*bottom*) antibodies as indicated.

directing the N terminus of Toc75 to the stroma and a polyglycine stretch mediating retrotranslocation to the intermembrane space (50, 51). The current working hypothesis assumes that only the transit peptide reaches the stroma and is cleaved off, whereas Toc75 remains assembled with the translocon (50). Although *pt*Omp85 does not possess a polyglycine stretch of comparable length, a triple-glycine motif can be found between the predicted transit peptide and the first POTRA domain (GGG at amino acids 90–92). The same motif can also be identified in the Omp85 homolog from the diatom *T. pseudonana* and in the Toc75 homolog from the free-living rhodophyte *C. merolae*. Consistent with its putative function in targeting, the triple-G motif is in close proximity to the predicted signal peptidase I cleavage site (AXA) (52).

To investigate the importance of the motif for Omp85 targeting, we generated fusion proteins of variable sequences derived from the *pt*Omp85 N terminus with GFP. All con-

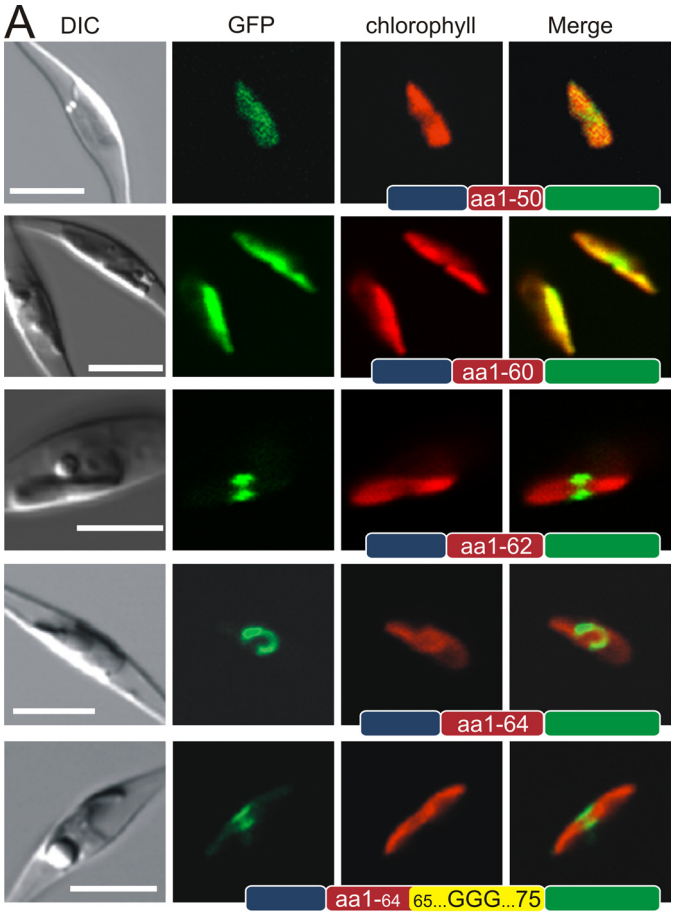

FIGURE 3. **Bipartite targeting signal of *pt*Omp85.** *A*, the signal peptide of 21 amino acids plus 50, 60, 62, 64, or 75 amino acids (*aa*; from *top* to *bottom*) fused to GFP was transfected into *P. tricornutum*. Shown are the differential interference contrast (*DIC*) image, GFP fluorescence, and chlorophyll fluorescence. *Merge* shows the overlay of chlorophyll and GFP fluorescence. The constructs are presented as a *bar*, where *blue* stands for the signal peptide, *red* for the transit peptide, *yellow* for the mature domain, and *green* for GFP. *Scale bars* = 5 μm. *B*, the hydrophobicity of the N-terminal 100 amino acids of *pt*Omp85 was calculated (ExPASy Proteomics Server ProtScale) in a sliding 9-amino acid window using the hydrophobicity scale established by Eisenberg *et al.* (53). The amino acid position was normalized to the phenylalanine at position 0. The N-terminal section of *pt*Omp85 is indicated as a *bar diagram* with the same coloring as in *A*. The *arrow* highlights the length of the sequence, where transition of GFP localization occurs.

structs contained the *pt*Omp85 signal peptide plus an additional 10–100 amino acids. We could show that all constructs containing the signal peptide and up to 60 additional amino acids (amino acids 1–60) were localized to the stroma of the complex plastid (Fig. 3*A*, *first* and *second panels*). In contrast, a construct containing just two additional amino acids (amino acids 1–62) directed GFP to a plastidal localization outside the stroma (*third panels*). Interestingly, the triple-glycine motif was not present in this construct, and the localization did not change when the polyglycine stretch was present (amino acids 1–75; *fifth panels*). These experiments defined the signal peptide plus the following 62 amino acids as the minimum targeting sequence that is necessary for correct *pt*Omp85 targeting.

These experiments showed that intraorganellar targeting of *pt*Omp85 is similar to the two-step targeting of Toc75 but is, in contrast to Toc75, not (or not exclusively) mediated by a glycine motif. Instead, the intraorganellar targeting might be mediated by means of hydrophobicity because we noted a conspicuous patch of 10 hydrophobic residues (Fig. 3*B*) using sliding window hydrophobicity analysis (53). However, this has to be analyzed in future studies using, for example, site-directed mutagenesis of the identified minimum targeting sequence.

N and C Termini of ptOmp85 Are Exposed to the PPC—Considering that *pt*Omp85 is a membrane protein (Fig. 2) and that it possesses a signal for stromal targeting comparable with that of Toc75 found in plants (Fig. 3), it appears likely that the protein is integrated in the third outermost membrane of the complex plastid. To confirm this hypothesis and to exclude a putative localization in the inner membrane, we applied the self-assembling split GFP system for *P. tricornutum*. Here, GFP was split into two fragments, S1–10 and S11. S1–10 represents β-strands 1–10 of the 11-stranded GFP β-barrel, and S11 represents the most C-terminal β-strand 11 (43). The individual fragments do not fluoresce but recover fluorescence by self-assembling if expressed simultaneously in the same cellular compartment, irrespective of their fusion partners (43).

First, we fused S11 to the C terminus of the mature *pt*Omp85 protein. When cells were cotransfected with a fusion of the PPC-targeted symbiontic Hsp70 BTS and S1–10, we observed fluorescence. This indicated that the C terminus of *pt*Omp85 was exposed to the PPC (Fig. 4*A*, *first panels*). The same result was observed when the PPC marker symbiontic Hsp70 BTS-S1–10 was cotransfected with a construct in which S11 was cloned into the putative N terminus of the mature *pt*Omp85 protein (*i.e.* between the putative signal peptidase I cleavage site and the first POTRA domain; *pt*pre-S11-Omp85) (*second panels*). To confirm our hypothesis, we cotransfected *pt*Omp85-S11 or *pt*pre-S11-Omp85 with the stroma-targeted AtpC BTS-S1–10 (Fig. 1*A*). In this case, we did not observe any fluorescence signal, which is consistent with retention of *pt*Omp85 in the intermembrane space during translocation as presumed for Toc75 (50).

Next, we used the MGD1 protein from *P. tricornutum* as a marker for the intermembrane space between the third and fourth membranes. In *Arabidopsis thaliana*, MGD1 is an intermembrane space-localized protein that is attached to but not inserted into the inner envelope (54, 55). Indeed, its fluorescence in *P. tricornutum* resembles a structure that might result from such localization (Fig. 4*B*). When *P. tricornutum* was cotransfected with *pt*Omp85-S11 and *pt*MGD1-S1–10, we could not observe any signal.

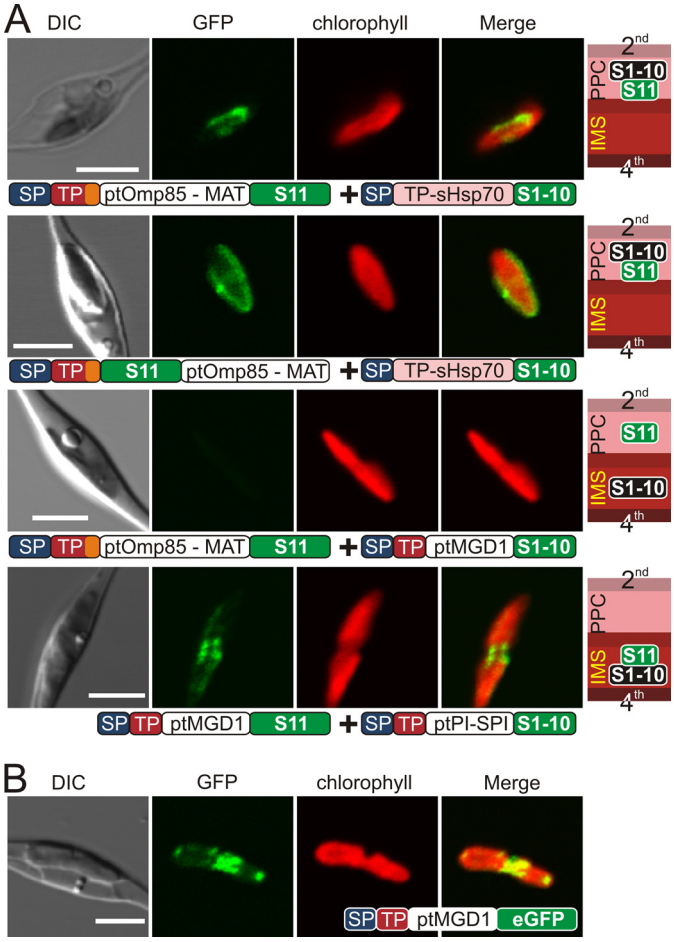

FIGURE 4. **Localization of *pt*Omp85 in the third outermost membrane.** *A*, the self-assembling split GFP system was adapted for *P. tricornutum*. Either of the two fragments of GFP (S1–10 or S11) was fused to *pt*Omp85 (S11, *first* and *third panels*), *pt*MGD1 (S1–10, *third panel*; and S11, *fourth panel*), or *P. tricornutum* plastidal type I signal peptidase I (S1–10, *third panel*) or was inserted between the BTS and mature domain of *pt*Omp85 (S11, *first* and *third panels*). The constructs that were cotransfected are shown below each panel. *Orange* indicates the hydrophobic region of the signal preceding the mature domain. Processing of the samples was performed as described in the legend to Fig. 2*B*. On the *right* site of each row, a model for the positioning of the two domains of the split GFP is given in the same color code as described in the legend to Fig. 1*A*. *MAT*, mature protein. *B*, *pt*MGD1 fused to GFP as presented in the *bar diagram* was cotransfected into *P. tricornutum*, and the processing of the samples was performed as described in the legend to Fig. 2*B*. *Scale bars* = 5 μm (*A* and *B*). *DIC*, differential interference contrast; *SP*, signal peptide; *TP*, transit peptide; *sHsp70*, symbiontic Hsp70; *IMS*, intermembrane space; *eGFP*, enhanced GFP.

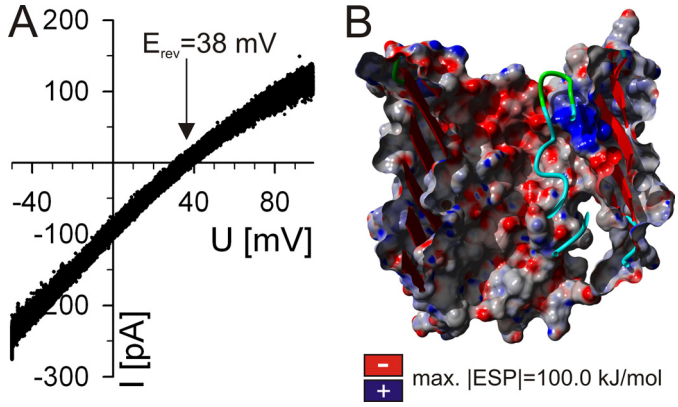

FIGURE 5. **Electrophysiological properties of *pt*Omp85: the reversal potential.** *A*, the reversal potential was determined by application of voltage ramps (ΔV = 10 mV/s) across bilayers (salt gradient of 250 to 20 mM KCl and 10 mM MOPS/Tris (pH 7), *cis*/*trans*). E_{rev} is an average of 45 independent experiments. *B*, the charge distribution of the channel interior not considering the integrated loop is shown. *Red* indicates acidic regions, and *blue* indicates basic regions. *ESP*, electrostatic potential.

While analyzing the genome of *P. tricornutum*, we identified another protein with putative function in protein translocation, namely a homolog of the plastidic signal peptidase I (>estExt_gwp_gw1.C_chr_10974, Department of Energy Joint Genomic Institute) (see supplemental Fig. 3 sequence alignment). In plant chloroplasts, the enzyme is localized in the thylakoids, where it processes signal peptides of thylakoidal proteins, and also in the intermembrane space, where it is involved in the processing of Toc75 (56). When we fused the *P. tricornutum* signal peptidase I homolog to S11 and coexpressed it in *P. tricornutum* with *pt*MGD1-S1–10, we observed a fluorescence signal (Fig. 4*A*, *fourth panels*) that was clearly distinct from a stromal localization (Fig. 2*A*). This confirms the intermembrane space localization of MGD1 and further suggests that the processing pathway of *pt*Omp85 is comparable with that of Toc75 from higher plants.

ptOmp85 Belongs to the Toc75-like Subfamily—Omp85 proteins have a β-barrel-shaped membrane domain (Fig. 1*C*), which generally shows a cation selectivity *in vitro* (27). We therefore analyzed the electrophysiological properties of the heterologously produced purified protein to determine the functional relation of *pt*Omp85 to one of the Omp85 family members. After reconstitution into liposomes and fusion of these with a planar bilayer for single-channel recording, we determined the reversal potential of the protein to be E_{rev} = 38 ± 1 mV (Fig. 5*A*), which reflects a permeability ratio of P_{K^+}/P_{Cl^-} = 6.9:1 and cation selectivity. These values correlate well with the behavior of Omp85 proteins analyzed previously (27) and with the acidic channel interior revealed by analyzing its charge distribution (Fig. 5*B*). Here, the negative charged residues are exposed to the channel interior, whereas the basic residues are covered by the internal loop typically found in Omp85 proteins (26).

Despite some similarities between Omp85 proteins, they are functionally distinct with respect to, for example, their function in membrane protein integration into the membrane (Sam50 type) or protein translocation across the membrane (Toc75 type). These functional differences are reflected in different values of the pore conductance of proteobacterial/mitochondrial Omp85 proteins on the one hand and cyanobacterial/plastidal Omp85 proteins on the other (27). Therefore, we determined the conductance of the pore formed by *pt*Omp85, as this has previously been shown to allow discrimination between Sam50- and Toc75-type Omp85 proteins (27). Analyses of the open and closed traces of the reconstituted channel showed several subconductance levels (Fig. 6*A*). Two main conductance states of *pt*Omp85 (g_{LARGE} = 467 ± 8 picosiemens and g_{SMALL} = 90 ± 6 picosiemens) could be observed (Fig. 5*B*). Consistent with previous results, the larger state showed further subconductance states ($g_{LARGE>}$ = 540 ± 20 picosiemens and $g_{LARGE<}$ = 360 ± 20 picosiemens) (Fig. 5*C*), and these values correspond to those of Omp85 from *Anabaena* sp. PCC 7120 and Toc75 of *Pisum sativum* (9, 17, 22). Using a corrected

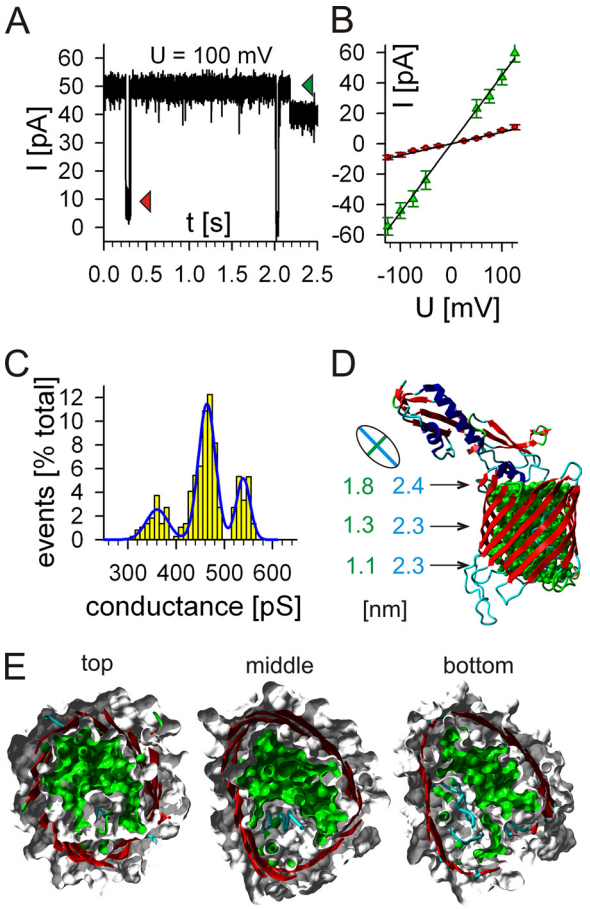

FIGURE 6. **Electrophysiological properties of *pt*Omp85: the conductance.** *A*, a representative current recording of a *pt*Omp85 bilayer at the indicated holding potential (250 mM KCl and 10 mM MOPS/Tris (pH 7), *cis/trans*) is shown, and the different subconductance states are marked. *B*, the current/voltage relationship of the two main conductance states (LARGE, *green*; SMALL, *red*) is shown. *C*, a histogram of subconductance states (conditions as described for *A*) is given. The distribution was analyzed by least-square fit to a 3-gauss equation. *pS*, picosiemens. *D*, the model for orientation of the cross-sections shown in *E* and the dimensions of the water-filled area are given. *E*, the cross-sections of the channel top, middle, and bottom are shown. The surface of the water molecules (*green*) and the protein (*gray*) and secondary structure elements are shown.

ohmic model (57), an approximation gives a pore diameter of 1.5 nm based on g_{LARGE}. This value is almost identical to the diameter calculated for *P. sativum* Toc75 (1.54 nm) and for Omp85 from *Anabaena* sp. (1.7 nm) and is thereby large enough to allow transport of unfolded polypeptide chains. The approximate diameter also corresponds to the structural properties of the protein deduced by homology modeling. According to the structural analysis, the most narrow region of the channel is located on the opposite site of the POTRA domain-containing surface (Fig. 6, *D* and *E*, *bottom*) and has a dimension of 2.3 ×1.1 nm. Approximating an elliptic structure, this would yield 2.0 nm^2, which is close to the 1.8 nm^2 determined by electrophysiological measurements.

DISCUSSION

The group Chromalveolata is thought to be monophyletic and is composed of the chromists and the alveolates (47). Many chromalveolates harbor so-called secondary plastids surrounded by more than two membranes. Accordingly, protein import into secondary plastids is considerably more complex than that into primary plastids. As initially postulated by Cavalier-Smith (47), the translocation machineries, which facilitate the passage of proteins across the plastid membranes, might have evolved only once and should therefore be indicators for the evolution of chromalveolates. Thus, studying protein transport into secondary plastids is not only of functional and mechanistic interest but is also indicative for the reconstruction of the evolutionary history of chromalveolates. Searching for possible translocons of secondary plastids surrounded by four membranes led to the identification of three candidates. These are Sec61 at the outermost membrane, the SELMA complex at the second outermost membrane, and a Tic complex at the innermost membrane (Fig. 1*A*) (3–5, 8, 58, 59). However, computational analyses of the genomes of chromalveolates failed to identify a convincing candidate translocon for the third outermost membrane. Our discovery of a membrane-inserted protein (Fig. 2) belonging to the Omp85 family (Fig. 1) in *P. tricornutum* may fill this gap.

The sequence of the newly identified protein is closely related to that of the Toc75 protein from the free-living red alga *C. merolae* (Fig. 1*B*). Additionally, all Omp85-like proteins from chromalveolates form an individual clade related to Toc75 from *C. merolae*, which is consistent with the current hypothesis that the plastids of chromalveolates share a common evolutionary origin (47). The electrophysiological properties of *pt*Omp85 with respect to cation selectivity (Fig. 5) and pore dimension (Fig. 6) support the phylogenetic classification as Toc75-type Omp85 protein (27). The determined pore size, also supported by the dimension of the homology model, would be sufficient for the translocation of an unfolded preprotein across a membrane (12). Hence, phylogenetic and physiological analyses strongly suggest a function for *pt*Omp85 in translocation.

Interestingly, Omp85 is not only phylogenetically related to Toc75 but also traffics to its target membrane in a mode similar to Toc75. Despite a characteristic phenylalanine at position +1 of the transit peptide, which is a signal for stromal import (6, 7), an additional intraorganellar targeting signal between the BTS and the POTRA domain of *pt*Omp85 (Fig. 3) was identified. The results of the split GFP analyses, which show that *pt*Omp85 exposes both termini toward the PPC (Fig. 4), and the observed two-step mode of targeting strongly argue for a localization of *pt*Omp85 in the third outermost plastid membrane. We therefore hypothesize that *pt*Omp85 is functionally orthologous to Toc75 and propose its function in protein import.

By sequence comparison, we additionally identified a protein with similarity to the peptidase involved in processing of Toc75 in higher plants (56), which is localized in the intermembrane space of the complex plastid based on the results obtained with the self-assembly GFP assay (Fig. 4 and Table 2). However, the thylakoid localization as observed in chloroplasts (56) cannot be excluded or confirmed by the chosen experimental strategy. Irrespective of a possible additional thylakoid localization of the peptidase, the mode of processing of *pt*Omp85 appears to be comparable between Toc75 from pea (50, 56) and Omp85 from *P. tricornutum.* This additionally implies that the complex translocation process of the plastidal Omp85 had evolved

TABLE 2

Split GFP analysis

Given are the proteins fused N-terminally to S1–10 (first column) or S11 (second column) of split GFP. The third column indicates whether fluorescence was detected, and the fourth column indicates the observed structure of the GFP signal. sHsp70, symbiontic Hsp70; sUbc4, symbiontic Ubc4; SHLP, stromal histone-like protein; PI-SPI, plastidal type I signal peptidase I; N-ter, N-terminal; C-ter, C-terminal; IMS, intermembrane space. "BTS" indicates that only the bipartite targeting sequence was used to target S1–10 to appropriate destinations; "FL" indicates that full-length open reading frames were cloned to S11.

S1–10 cloned to	S11 cloned to	Fluorescence	Location
sHsp70 BTS	sUbc4-FL	Yes	Blob
AtpC BTS	SHLP-FL	Yes	Stroma
sHsp70 BTS	SHLP-FL	No	
MGD1-FL	PI-SPI-FL	Yes	IMS
AtpC BTS	*pt*Omp-FL (N-ter)	No	
sHsp70 BTS	*pt*Omp-FL (N-ter)	Yes	Blob
sHsp70 BTS	*pt*Omp-FL (C-ter)	Yes	Blob
MGD1-FL	*pt*Omp-FL (C-ter)	No	
AtpC BTS	*pt*Omp-FL (C-ter)	No	

before the green and red algal lineages diverged, although the specific signals that mediate intraorganellar targeting differ slightly.

Although all results presented here indicate a function of *pt*Omp85 in transport, a functional proof is not currently possible, as conditional knock-outs cannot be generated in the diatom system. Hence, a final determination of the function of Omp85 of chromalveolates should be undertaken in genetically accessible organisms such as *T. gondii*. However, taking into account that (i) *pt*Omp85 is homologous to the proposed Toc75 of red alga, (ii) the electrophysiology and pore diameter of *pt*Omp85 are comparable with those of Omp85 proteins of cyanobacteria and Toc75 of land plants, and (iii) the cellular localization and targeting of *pt*Omp85 mirror that of Toc75, a function of *pt*Omp85 in protein translocation can be hypothesized.

Acknowledgments—We are grateful to the Geoff Waldo laboratory (Los Alamos National Laboratory, Los Alamos, NM) for providing templates for self-assembling GFP. We thank Jude Przyborski and Maik Sommer for help and critical reading of the manuscript.

REFERENCES

1. Field, C. B., Behrenfeld, M. J., Randerson, J. T., and Falkowski, P. (1998) *Science* **281,** 237–240
2. Winzeler, E. A. (2008) *Nature.* **455,** 751–756
3. Gould, S. B., Waller, R. F., and McFadden, G. I. (2008) *Annu. Rev. Plant Biol.* **59,** 491–517
4. Bolte, K., Bullmann, L., Hempel, F., Bozarth, A., Zauner, S., and Maier, U. G. (2009) *J. Eukaryot. Microbiol.* **56,** 9–15
5. Hempel, F., Bullmann, L., Lau, J., Zauner, S., and Maier, U. G. (2009) *Mol. Biol. Evol.* **26,** 1781–1790
6. Gruber, A., Vugrinec, S., Hempel, F., Gould, S. B., Maier, U. G., and Kroth, P. G. (2007) *Plant Mol. Biol.* **64,** 519–530
7. Gould, S. B., Sommer, M. S., Hadfi, K., Zauner, S., Kroth, P. G., and Maier, U. G. (2006) *J. Mol. Evol.* **62,** 674–681
8. van Dooren, G. G., Tomova, C., Agrawal, S., Humbel, B. M., and Striepen, B. (2008) *Proc. Natl. Acad. Sci. U.S.A.* **105,** 13574–13579
9. Schleiff, E., and Soll, J. (2005) *EMBO Rep.* **6,** 1023–1027
10. Löffelhardt, W., von Haeseler, A., and Schleiff, E. (2007) *Symbiosis* **44,** 33–42
11. Schnell, D. J., Kessler, F., and Blobel, G. (1994) *Science* **266,** 1007–1012
12. Hinnah, S. C., Wagner, R., Sveshnikova, N., Harrer, R., and Soll, J. (2002) *Biophys. J.* **83,** 899–911
13. Ruiz, N., Kahne, D., and Silhavy, T. J. (2006) *Nat. Rev. Microbiol.* **4,** 57–66
14. Gross, J., and Bhattacharya, D. (2009) *Nat. Rev. Genet.* **10,** 495–505
15. Thomas, W. R., and Rossi, A. A. (1986) *Infect. Immun.* **52,** 812–817
16. Ruffolo, C. G., and Adler, B. (1996) *Infect. Immun.* **64,** 3161–3167
17. Voulhoux, R., Bos, M. P., Geurtsen, J., Mols, M., and Tommassen, J. (2003) *Science* **299,** 262–265
18. Wu, T., Malinverni, J., Ruiz, N., Kim, S., Silhavy, T. J., and Kahne, D. (2005) *Cell* **121,** 235–245
19. Nicolaisen, K., Mariscal, V., Bredemeier, R., Pernil, R., Moslavac, S., López-Igual, R., Maldener, I., Herrero, A., Schleiff, E., and Flores, E. (2009) *Mol. Microbiol.* **74,** 58–70
20. Kozjak, V., Wiedemann, N., Milenkovic, D., Lohaus, C., Meyer, H. E., Guiard, B., Meisinger, C., and Pfanner, N. (2003) *J. Biol. Chem.* **278,** 48520–48523
21. Paschen, S. A., Waizenegger, T., Stan, T., Preuss, M., Cyrklaff, M., Hell, K., Rapaport, D., and Neupert, W. (2003) *Nature* **426,** 862–866
22. Gentle, I., Gabriel, K., Beech, P., Waller, R., and Lithgow, T. (2004) *J. Cell Biol.* **164,** 19–24
23. Baldwin, A., Wardle, A., Patel, R., Dudley, P., Park, S. K., Twell, D., Inoue, K., and Jarvis, P. (2005) *Plant Physiol.* **138,** 715–733
24. Hust, B., and Gutensohn, M. (2006) *Plant Biol.* **8,** 18–30
25. Kim, S., Malinverni, J. C., Sliz, P., Silhavy, T. J., Harrison, S. C., and Kahne, D. (2007) *Science* **317,** 961–964
26. Clantin, B., Delattre, A. S., Rucktooa, P., Saint, N., Méli, A. C., Locht, C., Jacob-Dubuisson, F., and Villeret, V. (2007) *Science* **317,** 957–961
27. Bredemeier, R., Schlegel, T., Ertel, F., Vojta, A., Borissenko, L., Bohnsack, M. T., Groll, M., von Haeseler, A., and Schleiff, E. (2007) *J. Biol. Chem.* **282,** 1882–1890
28. Konagurthu, A. S., Whisstock, J. C., Stuckey, P. J., and Lesk, A. M. (2006) *Proteins* **64,** 559–574
29. Kannan, N., Taylor, S. S., Zhai, Y., Venter, J. C., and Manning, G. (2007) *PLoS Biol.* **5,** e17
30. Bryson, K., McGuffin, L. J., Marsden, R. L., Ward, J. J., Sodhi, J. S., and Jones, D. T. (2005) *Nucleic Acids Res.* **33,** W36–W38
31. Mirus, O., and Schleiff, E. (2005) *BMC Bioinformatics* **6,** 254
32. Sali, A., and Blundell, T. L. (1993) *J. Mol. Biol.* **234,** 779–815
33. Krieger, E., Darden, T., Nabuurs, S. B., Finkelstein, A., and Vriend, G. (2004) *Proteins* **57,** 678–683
34. Canutescu, A. A., Shelenkov, A. A., and Dunbrack, R. L., Jr. (2003) *Protein Sci.* **12,** 2001–2014
35. Baker, N. A., Sept, D., Joseph, S., Holst, M. J., and McCammon, J. A. (2001) *Proc. Natl. Acad. Sci. U.S.A.* **98,** 10037–10041
36. Wang, J., Cieplak, P., and Kollmann, P. A. (2000) *J. Comp. Chem.* **21,** 1049–1074
37. Benson, D. A., Karsch-Mizrachi, I., Lipman, D. J., Ostell, J., and Wheeler, D. L. (2008) *Nucleic Acids Res.* **36,** D25–D30
38. Katoh, K., Kuma, K., Toh, H., and Miyata, T. (2005) *Nucleic Acids Res.* **33,** 511–518
39. Minh, B. Q., Vinh, L. S., von Haeseler, A., and Schmidt, H. A. (2005) *Bioinformatics* **21,** 3794–3796
40. Schmidt, H. A., Strimmer, K., Vingron, M., and von Haeseler, A. (2002) *Bioinformatics* 18, 502–504
41. Sommer, M. S., Gould, S. B., Lehmann, P., Gruber, A., Przyborski, J. M., and Maier, U. G. (2007) *Mol. Biol. Evol.* **24,** 918–928
42. Apt, K. E., Kroth-Pancic, P. G., and Grossman, A. R. (1996) *Mol. Gen. Genet.* **252,** 572–579
43. Cabantous, S., Terwilliger, T. C., and Waldo, G. S. (2005) *Nat. Biotechnol.* **23,** 102–107
44. Ertel, F., Mirus, O., Bredemeier, R., Moslavac, S., Becker, T., and Schleiff, E. (2005) *J. Biol. Chem.* **280,** 28281–28289
45. Wunder, T., Martin, R., Löffelhardt, W., Schleiff, E., and Steiner, J. M. (2007) *BMC Evol. Biol.* **7,** 236
46. Gardner, M. J., Hall, N., Fung, E., White, O., Berriman, M., Hyman, R. W., Carlton, J. M., Pain, A., Nelson, K. E., Bowman, S., Paulsen, I. T., James, K., Eisen, J. A., Rutherford, K., Salzberg, S. L., Craig, A., Kyes, S., Chan, M. S., Nene, V., Shallom, S. J., Suh, B., Peterson, J., Angiuoli, S., Pertea, M., Allen, J., Selengut, J., Haft, D., Mather, M. W., Vaidya, A. B., Martin, D. M.,

Fairlamb, A. H., Fraunholz, M. J., Roos, D. S., Ralph, S. A., McFadden, G. I., Cummings, L. M., Subramanian, G. M., Mungall, C., Venter, J. C., Carucci, D. J., Hoffman, S. L., Newbold, C., Davis, R. W., Fraser, C. M., and Barrell, B. (2002) *Nature* **419,** 498–511
47. Cavalier-Smith, T. (1999) *J. Eukaryot. Microbiol.* **46,** 347–366
48. Gould S. B., Sommer, M. S., Kroth, P. G., Gile, G. H., Keeling, P. J., and Maier, U. G. (2006) *Mol. Biol. Evol.* **23,** 2413–2422
49. Kilian, O., and Kroth, P. G. (2004) *J. Mol. Evol.* **58,** 712–721
50. Tranel, P. J., Froehlich, J., Goyal, A., and Keegstra, K. (1995) *EMBO J.* **14,** 2436–2446
51. Baldwin, A. J., and Inoue, K. (2006) *FEBS J.* **273,** 1547–1555
52. Tuteja, R. (2005) *Arch. Biochem. Biophys.* **441,** 107–111
53. Eisenberg, D., Schwarz, E., Komaromy, M., and Wall, R. (1984) *J. Mol. Biol.* **179,** 125–142
54. Miège, C., Maréchal, E., Shimojima, M., Awai, K., Block, M. A., Ohta, H., Takamiya, K., Douce, R., and Joyard, J. (1999) *Eur. J. Biochem.* **265,** 990–1001
55. Benning, C., and Ohta, H. (2005) *J. Biol. Chem.* **280,** 2397–2400
56. Inoue, K., Baldwin, A. J., Shipman, R. L., Matsui, K., Theg, S. M., and Ohme-Takagi, M. (2005) *J. Cell Biol.* **171,** 425–430
57. Smart, O. S., Breed, J., Smith, G. R., and Sansom, M. S. (1997) *Biophys. J.* **72,** 1109–1126
58. Spork, S., Hiss, J. A., Mandel, K., Sommer, M., Kooij, T. W., Chu, T., Schneider, G., Maier, U. G., and Przyborski, J. M. (2009) *Eukaryot. Cell* **8,** 1134–1145
59. Kalanon, M., Tonkin, C. J., and McFadden, G. I. (2009) *Eukaryot. Cell* **8,** 1146–1154